Journal of Biomechanics 53 (2017) 97–104

Contents lists available at ScienceDirect

Journal of Biomechanics

journal homepage: www.elsevier.com/locate/jbiomech
www.JBiomech.com

Experimental evaluation of a new morphological approximation of the articular surfaces of the ankle joint

Claudio Belvedere [a], Sorin Siegler [b,*], Andrea Ensini [c], Jason Toy [b], Paolo Caravaggi [a], Ramya Namani [b], Giulia Giannini [a], Stefano Durante [d], Alberto Leardini [a]

[a] Movement Analysis Laboratory, Istituto Ortopedico Rizzoli, Bologna, Italy
[b] Department of Mechanical Engineering and Mechanics, Drexel University, Philadelphia, PA, USA
[c] 1st Orthopaedic-Traumatologic Clinic, Istituto Ortopedico Rizzoli, Bologna, Italy
[d] Nursing, Technical and Rehabilitation Assistance Service, Istituto Ortopedico Rizzoli, Bologna, Italy

ARTICLE INFO

Article history:
Accepted 3 January 2017

Keywords:
Ankle
Morphology
Approximation
Kinematics
In vitro

ABSTRACT

The mechanical characteristics of the ankle such as its kinematics and load transfer properties are influenced by the geometry of the articulating surfaces. A recent, image-based study found that these surfaces can be approximated by a saddle-shaped, skewed, truncated cone with its apex oriented laterally. The goal of this study was to establish a reliable experimental technique to study the relationship between the geometry of the articular surfaces of the ankle and its mobility and stability characteristics and to use this technique to determine if morphological approximations of the ankle surfaces based on recent discoveries, produce close to normal behavior. The study was performed on ten cadavers. For each specimen, a process based on medical imaging, modeling and 3D printing was used to produce two subject specific artificial implantable sets of the ankle surfaces. One set was a replica of the natural surfaces. The second approximated the ankle surfaces as an original saddle-shaped truncated cone with apex oriented laterally. Testing under cyclic loading conditions was then performed on each specimen following a previously established technique to determine its mobility and stability characteristics under three different conditions: natural surfaces; artificial surfaces replicating the natural surface morphology; and artificial approximation based on the saddle-shaped truncated cone concept. A repeated measure analysis of variance was then used to compare between the three conditions. The results show that (1): the artificial surfaces replicating natural morphology produce close to natural mobility and stability behavior thus establishing the reliability of the technique; and (2): the approximated surfaces based on saddle-shaped truncated cone concept produce mobility and stability behavior close to the ankle with natural surfaces.

1. Introduction

Total ankle replacement (TAR) is becoming a common surgical procedure for treatment of end-stage ankle osteoarthritis. This is primarily due to a number of drawbacks of the traditional alternative, i.e. ankle arthrodesis, including limited mobility and development of adjacent joint arthritis (Coester et al., 2001). However, while total hip and knee joint replacements have become the treatment of choice for end-stage osteoarthritis, with very low failure rates and few clinical complications, TAR is still plagued by lower survival rates (Spirt et al., 2004). The ability to reproduce the natural motion of the intact joint has been recognized as key factor for the success of implants for joint replacement. However, the surface morphology and the associated kinematics of the ankle joint are three dimensional (3D) and complex (Siegler et al., 1988; Lundberg et al., 1989; Leardini et al., 1999). A major challenge in TAR is designing and manufacturing artificial joint surfaces able to approximate this complex morphology and kinematics, and requires careful analysis of the functional morphology of the natural articular surfaces to identify their essential features.

Some of the pioneering studies on the functional morphology of the talar dome were conducted more than 60 years ago and included the seminal work by Inman and Close and their co-workers (Sewell, 1904; Barnett and Napier, 1952; Close and Inman, 1952; Hicks, 1953; Close, 1956). At that time, most investigators regarded the ankle joint as a one-degree of freedom joint with a fixed axis of rotation. Relying on this single axis assumption, direct morphological measurements of the talar

* Correspondence to: Department of mechanical Engineering and Mechanics, Drexel University, 32nd and Chestnut Streets, Philadelphia, PA 19104, USA. Fax: +1 215 895 1478.
E-mail address: ssiegler@coe.drexel.edu (S. Siegler).

http://dx.doi.org/10.1016/j.jbiomech.2017.01.002
0021-9290/

dome and the distal tibia were performed in cadaver specimens (Close and Inman, 1952; Close, 1956; Inman, 1976). It was concluded that the trochlear surface of the talus can be approximated as a frustum of a cone, whose apex is directed medially and whose axis of revolution coincides with the line connecting the tips of the medial and lateral malleolus (Close and Inman, 1952; Inman, 1976). Relying on the validity of this postulate, the articulating surfaces of some TAR systems incorporate the truncated cone with medal apex geometry. More recently, an image-based 3D study was conducted on the morphology of the ankle joint surfaces (Siegler et al., 2014). In this study, no kinematic constraints, either translational or rotational, such as a fixed axis of rotation, were imposed. 3D models of the talus and of the tibia were produced from computer tomography (CT) images. From these models a number of geometric measurements were performed from which geometrical approximations could be produced. It was concluded that the trochlear surface of the talus, and the articulating tibial surface, can be approximated by a skewed truncated conic saddle shape, with its apex oriented laterally. These novel results were different from those reported previously (Close and Inman, 1952; Inman, 1976), and were demonstrated to be due to the fact that, unlike those early studies, no fixed axis rotation constraint was imposed.

Different geometrical approximations of the articular surfaces of the ankle may have different effects on its mechanical behavior, such as kinematic properties and load transfer characteristics. Therefore, TARs with different surface geometries may produce different ankle behavior possibly leading to significant differences in long term outcomes such as failure rates. Therefore, the first major goal of the present study was to develop and test the reliability of an in vitro experimental procedure to investigate the effect of different surface joint morphologies on the mobility and stability characteristics of the ankle. The procedure was based on producing specimen-specific 3D computer models of the articulating bones from CT scans and using these models to design and produce specimen-specific 3D printed implants. These implants were then surgically implanted and tested in the same specimens. In order to test the reliability of the technique, implant sets with artificial surfaces replicating the corresponding natural surfaces were produced and tested. The second major goal of the study was to use this technique to determine whether the implantable artificial approximation of the anatomical joint surfaces proposed recently by Siegler et al. (Siegler et al., 2014) produces mobility and stability characteristics similar to those of the natural surfaces.

2. Methodology

2.1. Summary

The experimental procedure was designed to study in-vitro the effect of different ankle surface morphologies on its mobility and stability characteristics. In this study, “mobility” is defined as the angular joint's rotation and range of motion in three planes. Stability refers to the total joint laxity which is here defined as the ratio between the range of motion in degrees in a given direction (inversion/eversion or internal/external rotation) and the total torque required to produce it. The entire process was performed on each specimen, and consisted of the following steps: pre-testing surgical preparation and CT imaging; image processing, modeling, designing and 3D printing of artificial surfaces; mechanical testing of the original intact specimen; surgical removal of the natural surfaces and implantation of the 3D printed artificial components; and repetition of the mechanical testing with each set of artificial surfaces.

2.2. Pre-testing surgical preparations and CT imaging

Ten fresh-frozen legs from below knee cadaveric dissections were used in this study. The specimens were obtained from ten subjects, three females and seven males, with an age range of 18–77 years old and an average age of 47. Each specimen was thawed for at least 24 h at room temperature. It was carefully inspected clinically and radiologically and inspected again during the subsequent surgical preparation for any observable defects or deformities. During these inspections, the integrity of ligaments and of the articular surfaces was verified. The entire surgical preparation and implantation procedure described below was performed by an orthopedic foot and ankle surgeon with large clinical experience in TAR. Using a standard anterior surgical approach, the articular surfaces were exposed. A standard surgical instrumentation jig used routinely for implantation of a currently available TAR was fixed to the distal tibia with the foot in neutral position, and with the extra-medullary rod of the jig aligned with the long axis of the tibia in both the sagittal and coronal planes (Giannini et al., 2010). The proper size tibial cutting block was selected and centered medio-laterally in the ankle mortise, providing the means to drill two parallel tunnels in the distal tibia. These tunnels were later used to fix the tibial components of the artificial surfaces as well as to provide clearly identifiable references. Three 2 mm diameter holes approximately 5 mm deep from the surface of the bones were then drilled into the tibia, talus, and calcaneus, and were used as fiduciary markers for registration. The specimen was then CT scanned (Brilliance CT 16-slice system by Philips Healthcare, DA Best, The Netherlands) with an in-plane resolution of 0.15 mm and a 0.4 mm inter-slice distance (Fig. 1a). The leg was then re-frozen while waiting for the design and production of the 3D printed artificial components.

2.3. Image processing, modeling, designing and 3D printing

The data from the CT scans (Fig. 1a) stored via Digital Imaging and Communications in Medicine (DICOM) were imported into an image processing software (Analyze Direct™, Overland Park, KS-USA) to obtain, after proper segmentation, 3D filtering and rendering, a 3D representation of the articulating bones including the tibia, fibula, talus and calcaneus (Fig. 1b). The stereo lithography (STL) files containing these 3D models of the bones were then imported into a reverse engineering program (Geomagic™, Morrisville, NC-USA) where they were further processed and where all the necessary dimensions required for the design of the artificial surfaces were performed (Fig. 1c). Two sets of these implantable surfaces were used in the study. Each set consisted of a tibial and a talar component with matching articulating surfaces. A uniform offset of 1.5 mm was introduced to account for the articular cartilage layer that was not visualized in the CT images. This value was based on an approximate average joint spacing observed in the CT images for the specimens. One implantable set consisted of articular surfaces that replicated the natural surfaces as obtained from the CT scan. This set was referred to as the ANATOMICAL set (Fig. 1d, left). The second set (Fig. 1d, right) consisted of the approximation to the natural surfaces (Siegler et al., 2014) consisting of a saddle shaped skewed truncated cone with the apex of the cone oriented laterally (from now on, referred to as SSCL). The attachment of the tibial component to the distal tibia was designed to include two 5 mm diameter cylinders that were fit into the two previously prepared 5 mm diameter tunnels in the distal tibia. A small plate in front of this component provided a means to temporarily secure the tibial

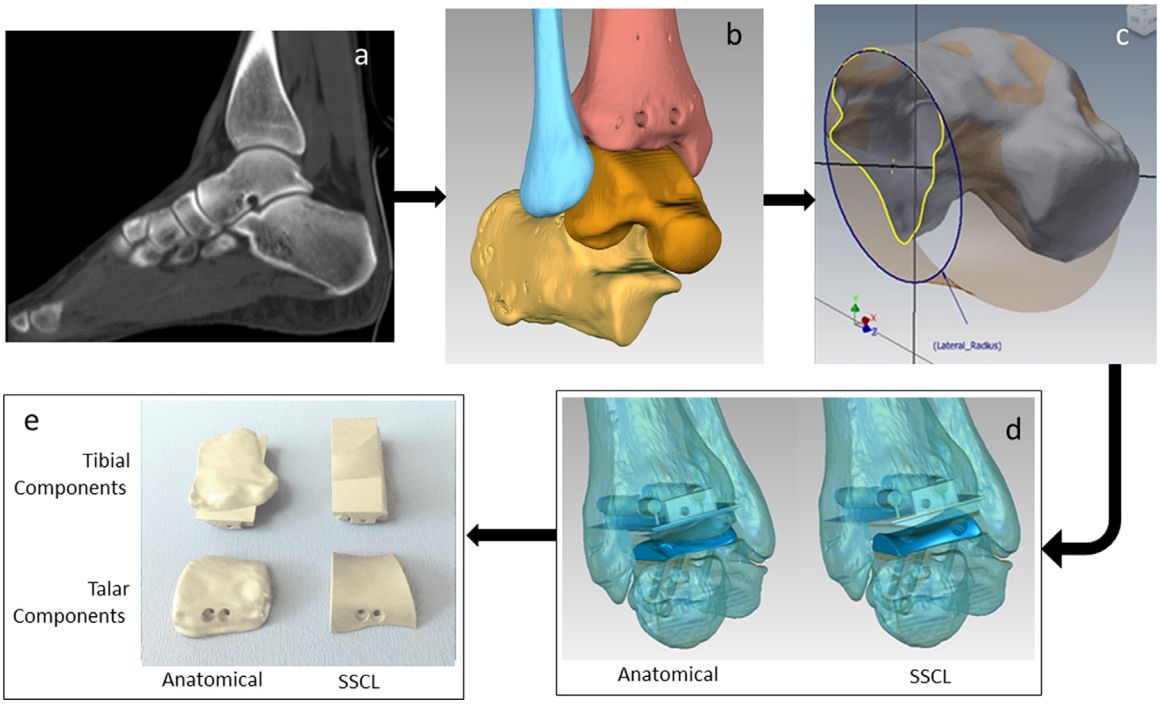

Fig. 1. Images for the process from CT imaging to 3D printed surface sets: a – CT slice image showing the bones to be segmented; b – 3D rendering of the four relevant bones, front view; c – one of the measurements performed on the talar bone model, to produce the skewed truncated cone with the apex of the cone oriented laterally (SSCL) surface approximation; d – 3D rendering of the talar and tibial components of the anatomical (left) and SSCL (right) surfaces once implanted in the corresponding bones; e – view of the 3D printed implant sets: the anatomical (left) and SSCL (right).

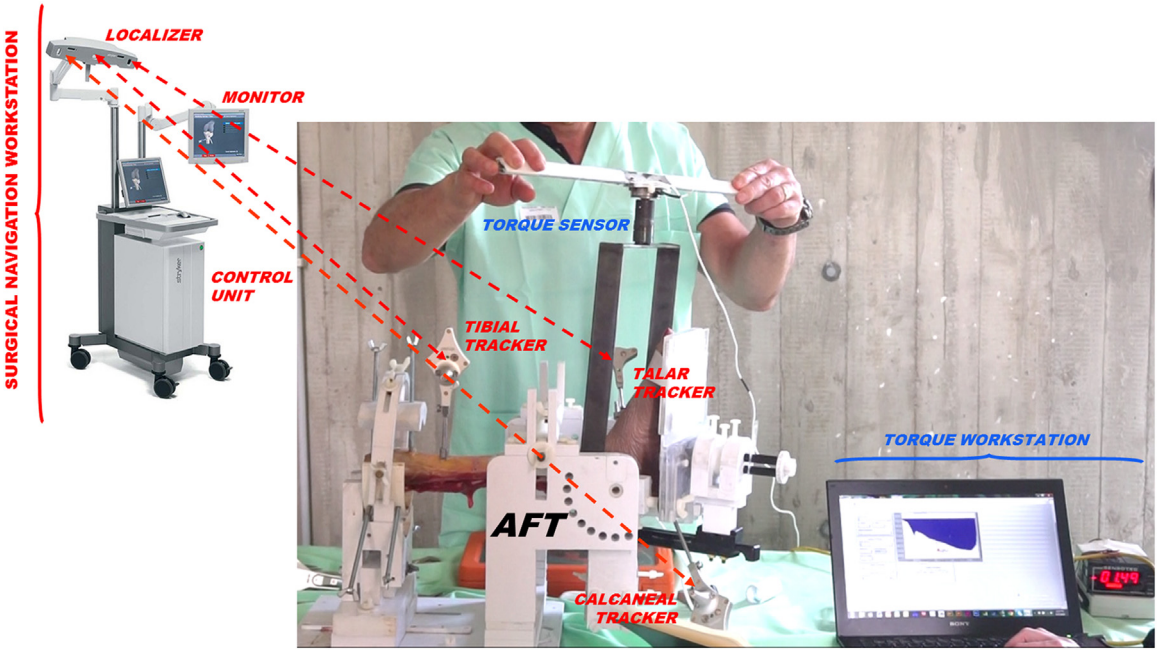

Fig. 2. Experimental setup showing testing of one cadaver specimen. The specimen is aligned and fixed in the AFT. Loading is applied manually and recorded through a torque sensor. Motion produced at the ankle, subtalar, and ankle complex is recorded by the optoelectronic kinematic data acquisition system (Surgical Navigation Workstation) through its three bone trackers.

component for the duration of the test. The talar component had two holes allowing the temporary fixation to the talus by corresponding screws. The design of these fixation elements (Fig. 1d) was such as to allow an easy removal of the implants after completing the relevant test and their replacement by the other set of implants on the same specimen. The design of the two sets of implants was conducted in Inventor™ (by Auto-Desk, San Rafael, CA-USA). The STL files representing the 3D models of the implants were then sent to a 3D printer (Dimensions Elite™ by Stratasys, Inc.) that produced the corresponding implant prototypes in acrylonitrile butadiene styrene with a spatial resolution of 0.2 mm (Fig. 1e). In

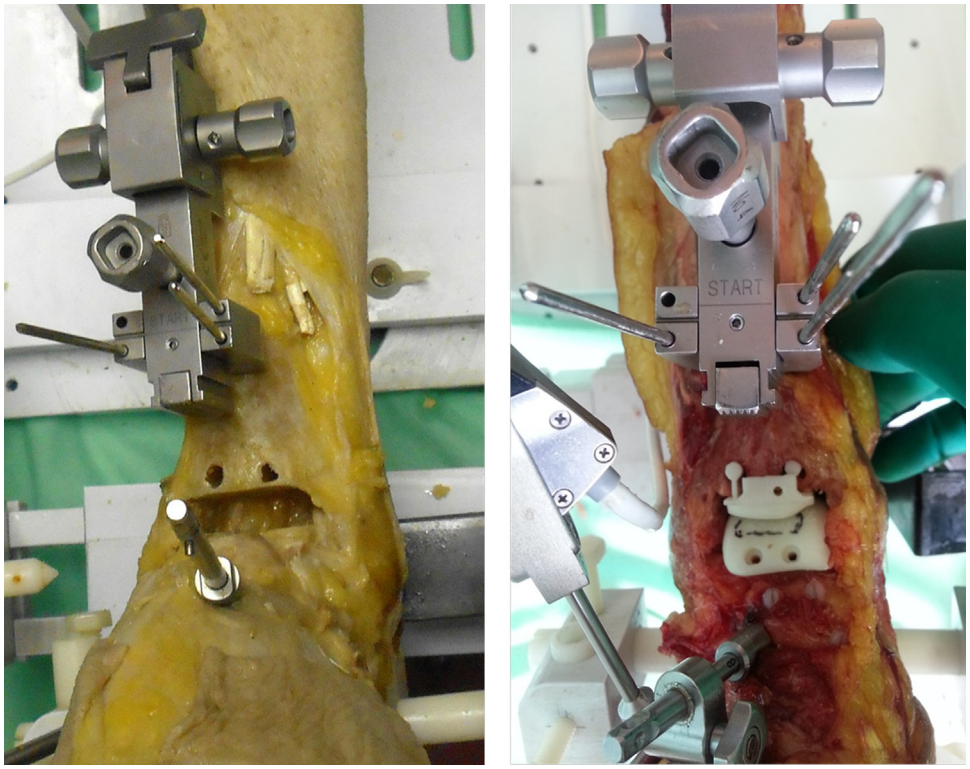

Fig. 3. Frontal views of one specimen before (left) and after (right) the surgical implantation of the 3D printed artificial components. The distal part of the alignment jig in shown attached to the tibia.

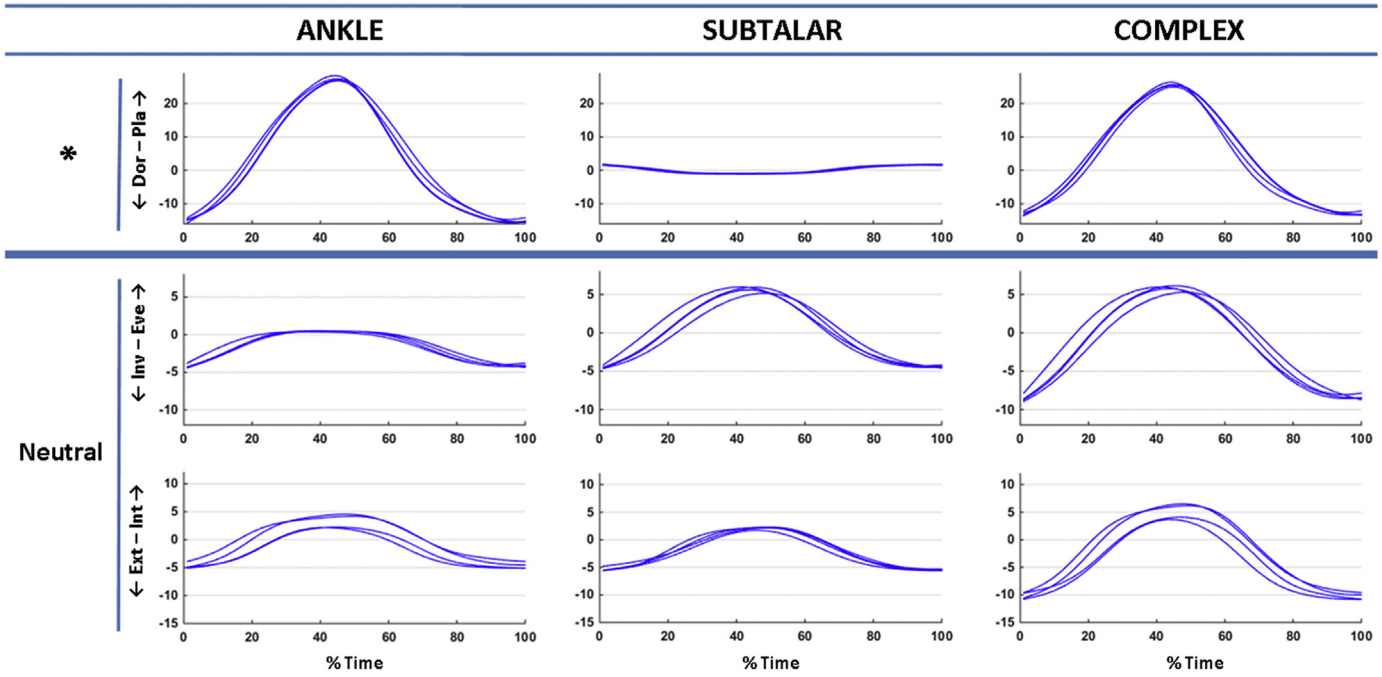

Fig. 4. Joint rotations (in degrees) obtained from four repetitions in an intact representative specimen, showing the cycle-to-cycle, intra-subject variability in the kinematic data. The cycle time was normalized to a range of 0–100%. Dorsiflexion–Plantarflexion (Dor–Pla) is reported for the full range of flexion (*no torque sensor used in this direction) and for motion produced through torque application in inversion–eversion (Inv–Eve) and internal–external rotation (Int–Ext) starting from the neutral.

addition, the cylindrical holes (three in each bone) used as fiduciary markers, were identified and segmented. The coordinates of the points of intersection of the symmetry axis of these cylinders and the surface of the bones were recorded and used for registration of the bones to the positional data recorded during the tests.

2.4. Testing and re-testing

A series of tests were conducted on each specimen to determine its mechanical response under controlled applied loads under each of the three conditions, starting with the natural surfaces (NATURAL), proceeding with the ANATOMICAL artificial

Table 1
The primary kinematics (in degrees) and torques (in Nm) at the ankle, subtalar and complex joints. Dorsiflexion–Plantarflexion (Dor–Pla) is reported for the full range of flexion (*no torque sensor used in this direction); Motion produced through torque application in inversion–eversion (Inv–Eve) and internal–external rotation (Int–Ext) start from the Neutral, maximum dorsiflexion (MaxDorsi) and maximum plantarflexion (MaxPlantar) joint positions. Data reported include the mean and standard deviations (SD) of the range of motion at the ankle, subtalar, and ankle complex for the NATURAL specimens and after the implantation of the artificial ANATOMICAL and SSCL sets.

			NATURAL		*ANATOMICAL*		*SSCL*	
			Mean	**(SD)**	**Mean**	**(SD)**	**Mean**	**(SD)**
*	**Dor–Pla**	**ANKLE**	40.3	(8.4)	39.7	(9.2)	42.2	(11.0)
		SUBTALAR	3.0	(1.9)	2.3	(0.7)	2.4	(1.4)
		COMPLEX	38.9	(7.6)	39.2	(8.3)	41.4	(8.8)
		TORQUE	–	–	–	–	–	–
Neutral	**Inv–Eve**	**ANKLE**	7.6	(7.0)	9.3	(10.1)	9.8	(10.6)
		SUBTALAR	12.2	(5.0)	13.1	(4.9)	12.7	(3.5)
		COMPLEX	16.6	(4.3)	17.9	(6.7)	17.5	(5.9)
		TORQUE	11.5	(1.5)	12.3	(2.4)	12.7	(2.3)
	Ext–Int	**ANKLE**	14.0	(9.7)	17.6	(8.6)	17.9	(9.2)
		SUBTALAR	12.2	(6.8)	11.7	(6.5)	11.5	(6.4)
		COMPLEX	24.9	(5.3)	27.6	(7.7)	28.5	(9.1)
		TORQUE	8.7	(1.7)	8.0	(1.8)	6.1	(1.7)
MaxDorsi	**Inv–Eve**	**ANKLE**	4.2	(6.3)	5.8	(8.0)	6.1	(6.2)
		SUBTALAR	8.3	(4.2)	8.9	(3.6)	8.2	(4.1)
		COMPLEX	9.1	(3.7)	10.5	(3.7)	11.1	(5.1)
		TORQUE	11.9	(1.5)	11.8	(2.0)	11.3	(2.2)
	Ext–Int	**ANKLE**	7.5	(5.9)	13.5	(8.2)	14.2	(10.1)
		SUBTALAR	9.3	(5.9)	7.8	(5.2)	7.1	(5.3)
		COMPLEX	13.4	(6.8)	18.6	(7.9)	18.9	(10.2)
		TORQUE	10.4	(2.3)	9.8	(1.4)	8.7	(1.5)
MaxPlantar	**Inv–Eve**	**ANKLE**	9.5	(6.2)	11.3	(10.3)	10.4	(9.2)
		SUBTALAR	11.8	(5.1)	10.2	(3.3)	10.0	(3.7)
		COMPLEX	18.7	(5.5)	17.3	(6.6)	15.9	(6.4)
		TORQUE	10.7	(1.8)	11.2	(2.3)	11.2	(2.1)
	Ext–Int	**ANKLE**	14.1	(9.4)	15.0	(8.9)	14.0	(7.3)
		SUBTALAR	14.0	(10.1)	12.1	(7.8)	11.6	(7.5)
		COMPLEX	28.5	(4.6)	27.1	(7.7)	26.1	(7.1)
		TORQUE	9.7	(1.9)	9.7	(2.2)	8.8	(1.7)

surfaces and concluding with the SSCL artificial surfaces. For this purpose, a six-degrees-of-freedom linkage, referred to as the Ankle Flexibility Tester (AFT), in conjunction with an optoelectronic stereo-photogrammetric motion data acquisition system (Stryker Knee Navigation System, Stryker®, Kalamazoo, MI-USA; nominal accuracy: 0.5 mm and 0.5 degrees) were used. The AFT was validated and used in previous in-vitro (Lapointe et al., 1997; Imhauser et al., 2002; Ringleb et al., 2005; Imhauser et al., 2008) and in-vivo (Siegler et al., 1996; Lapointe et al., 1997; Siegler et al., 1997; Liu et al., 2001; Siegler et al., 2005) studies. The device provides the capability to apply and measure continuous torques across the ankle complex while measuring the motion produced in response at the ankle, subtalar, and ankle complex. Simultaneously with the application of the torques, the optoelectronic system was utilized to track the motion of the bones (tibia, talus, and calcaneus). The optoelectronic system previously used in computer aided surgery (Sparmann et al., 2003; Belvedere et al., 2014) and adapted for small joint tracking (Belvedere et al., 2007; Franci et al., 2009; Belvedere et al., 2014; Sancisi et al., 2014) (Fig. 2) consisted of a camera sensor and a computer with dedicated software, and four trackers with 5 light-emitting-diodes each, capable of recording the motion of a rigid body object in space. Three trackers were securely fixed to the tibia, talus and calcaneus to record their corresponding motion. The fourth tracker was used for system control and landmark digitization.

In the first test, motion was produced over the entire range of motion of the ankle complex in flexion/extension by manually loading the foot plate of the AFT with a torque in the sagittal plane, without the use of the torque sensor. No torque sensor was used due to the large flexibility of the joint complex in this rotational direction. In the subsequent tests, motion was produced at the ankle complex by manually applying torques through an instrumented torque sensor about the inversion/eversion and internal/external rotation axes of the AFT (Siegler et al., 1996). These torques were applied starting from three different joint positions within the flexion arc, i.e. the neutral (Neutral), the maximum dorsiflexion (MaxDorsi), and maximum plantarflexion (MaxPlantar). At least four loading-unloading cycles were applied in each test at a slow rate of approximately 5 cycles per minute. Simultaneously with the application of the torques, the optoelectronic system was utilized to track the motion of the bones (tibia, talus, and calcaneus).

Following testing of the ankle with natural surfaces (NATURAL), with the specimen still secured to the AFT, the surgeon performed the bone preparation for artificial surface implantation. Particularly, the two reference parallel holes in the distal tibia were used to re-align the cutting jig, and with the foot in neutral position, the

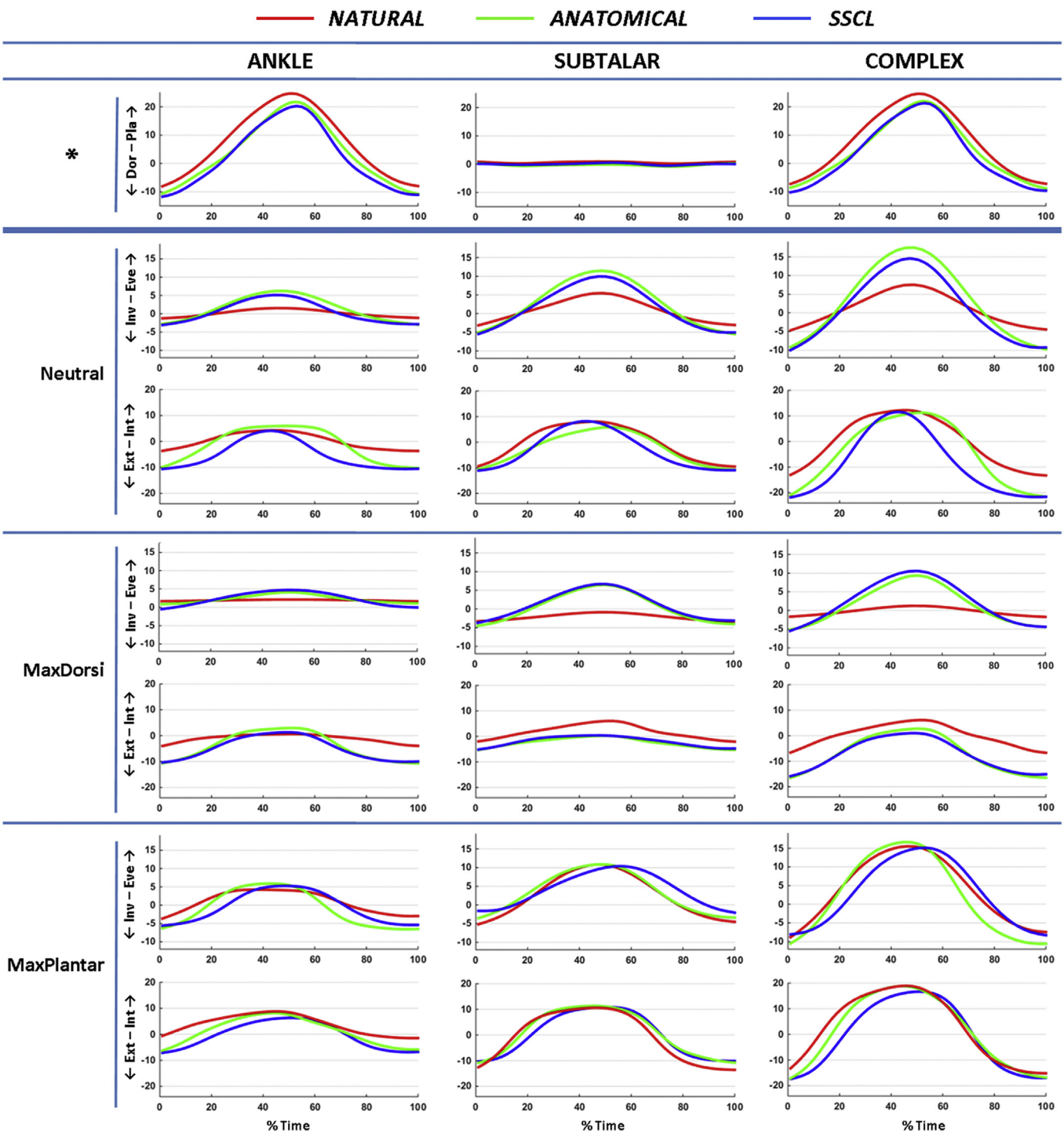

Fig. 5. Cycle-to-cycle average kinematics for the ankle joint, subtalar joint, and ankle complex obtained from one representative specimen before (NATURAL) (red) and after the implantation of the artificial ANATOMICAL (green) and SSCL (blue) sets. Dorsiflexion–Plantarflexion (Dor–Pla) is reported for the full range of flexion (*no torque sensor used in this direction); Motion produced through torque application in inversion–eversion (Inv–Eve) and internal–external rotation (Int–Ext) start from the Neutral, maximum dorsiflexion (MaxDorsi) and maximum plantarflexion (MaxPlantar) joint positions.(For interpretation of the references to color in this figure legend, the reader is referred to the web version of this article.)

tibial and talar cuts were performed. The ANATOMICAL set was then implanted into the distal tibia using the two 5 mm diameter cylinders and secured in place with the 2 mm diameter screws (Fig. 3). The previous loading conditions were then repeated. The ANATOMICAL set was then removed and the SSCL set was positioned on the same bone cuts using the same fixation elements, and the same loading conditions were repeated.

Testing of each specimen was concluded by digitization of the fiduciary markers described earlier using the fourth tracker of the optoelectronic system, i.e. the digitizer. For this purpose, the location of the center of each fiduciary hole on the surface of the bone was identified and digitized. In addition, still using the same digitizer, the location of a number of anatomical landmarks were recorded including the tibial tuberosity and the two malleoli, the

Table 2
The primary total laxity in degrees per newton meters of the ankle complex in inversion/eversion and internal/external rotation. Data reported include the mean and standard deviations (SD) of the total laxity of the ankle complex for the NATURAL specimens and after the implantation of the artificial ANATOMICAL and SSCL sets.

		NATURAL		*ANATOMICAL*		*SSCL*	
		Mean	**(SD)**	**Mean**	**(SD)**	**Mean**	**(SD)**
Neutral	**Inv–Eve**	1.5	(0.5)	1.6	(0.4)	1.7	(0.5)
	Ext–Int	3.0	(0.9)	3.5	(1.5)	4.5	(1.2)
MaxDorsi	**Inv–Eve**	0.7	(0.4)	0.9	(0.2)	1.0	(0.3)
	Ext–Int	1.3	(0.5)	1.9	(0.8)	1.5	(0.5)
MaxPlantar	**Inv–Eve**	1.8	(0.5)	1.5	(0.6)	1.5	(0.4)
	Ext–Int	2.7	(0.4)	2.8	(1.2)	3.0	(1.1)

four corners on the talar horizontal osteotomy, and, on the calcaneus, the Achilles's tendon insertion, the central plantar and the most prominent lateral facet.

2.5. Data processing

The digitized anatomical landmarks were used to establish anatomical reference frames for the tibia/fibula, talus, and calcaneus (Cappozzo et al., 1995) and the motion between these frames was used to assess kinematics at the tibio-talar (ankle), talo-calcaneal (subtalar), and tibio-calcaneal (complex) joints. For each of these, dorsiflexion/plantarflexion (Dor–Pla), inversion/eversion (Inv–Eve) and internal/external rotation (Int–Ext) movements were calculated according to a joint coordinate system convention (Grood and Suntay, 1983). Primary kinematics were defined as the joint rotation produced in the direction of the applied torque, while coupled kinematics were defined as the two other joint rotations. For each specimen and testing condition, intra-specimen kinematic data were collected to test motion reproducibility over the loading-unloading cycles, both for the primary and for the coupled kinematics. The time of each loading-unloading cycle was normalized to 0–100% to allow cycle-to-cycle statistical analysis. The reproducibility was defined as the largest standard deviation (SD) over the cycle period. The intra-specimen variability was also calculated for the applied torques.

Rotational range of motion, torques required to produce these ranges, and corresponding total laxity values were calculated for all testing conditions and for each of the three articulating surface configurations, i.e. the NATURAL, ANATOMICAL and SSCL sets. The differences in primary rotational range of motion and in total laxity in inversion/eversion and internal/external rotation between these configurations were tested for significance using repeated-measure multifactor analysis of variance, significance being accepted at $p < 0.05$.

3. Results

Small data variability in cycle-to-cycle kinematics at the ankle, subtalar and complex joints was found for all specimens (Fig. 4). The maximum standard deviation of the primary and coupled joint rotation patterns in all directions and for all specimens was smaller than 2.0 deg. In addition, the cycle-to-cycle variability in the applied torque was smaller than 0.3 Nm. This applies to the ankle with natural surfaces as well as to the ankle with the two artificial sets of surfaces. Inter-specimen variability in the ranges of motion and in the corresponding ranges of applied torques (Table 1) was larger than intra-specimen variability.

The repeated measure multi-parametric ANOVA revealed no statistical significance between the three different joint surface conditions, i.e. the NATURAL, ANATOMICAL and SSCL sets for either the ranges of motion or for the total laxity values. However, differences in the patterns of motion between the three joint surface conditions were qualitatively observed (Fig. 5). Also the kinematic patterns produced by the SSCL set, are qualitatively observed to closely follow those of the ANATOMICAL set (Fig. 5). Finally, the repeated measure multi-parametric ANOVA performed on the total laxity values in inversion/eversion and internal/external rotation showed that these values decrease significantly when the ankle is in dorsiflexion compared to neutral (Table 2). No such significant change was observed in plantarflexion when compared to neutral (Table 2).

4. Discussion and conclusions

Many TAR systems are currently in clinical use but, unlike current total hip and knee replacements, they suffer from unacceptable high, long-term failure rates, (Wood et al., 2000; Hintermann et al., 2004). Therefore, designing improved TARs with lower failure rates represents a significant contemporary engineering challenge. Clearly, the long-term, post-operative clinical outcome study is the ultimate determinant of the success of a specific TAR design. However, such studies are statistical in nature and subject to large inter-subject variability problems. They also fail to provide direct associations between specific TAR features and relevant in-situ function, such as mobility and stability properties or load transfer characteristics. In order to assist in overcoming the TAR design challenges, as well as to compare the biomechanics of different TARs, it is important to set-up a reliable experimental technique allowing to determine the relationship between specific TAR features, such as surface morphology, and the kinematic or load transfer characteristics. Objective in vitro studies comparing the kinematic function of different TARs were reported in the past (Valderrabano et al., 2003a, 2003b, 2003c). However, these included off-the-shelf commercial TARs and were not customized to the specific morphology of the tested specimens. Moreover, the artificial replica of the specific ankle joint surface morphology has never been included, whereas, in the present study such inclusion provided a unique opportunity to assess the reliability of the overall procedure. The latter combines medical imaging, image processing, 3D modeling, and 3D printing, with an established in vitro experimental setup to study the effect of joint surface morphology on joint's mobility and stability. Furthermore, all 3D printed implantable sets could be tested and compared in each single specimen, resulting in a powerful repeated measure ANOVA design which eliminates the known effect of the high inter-subject variability.

The reliability of the experimental technique was evaluated in two ways. First, the intra-specimen cycle-to-cycle variability, in both range of motion and in the torque required to produce it, were small (less than 2 degrees and less than 0.3 Nm respectively). Second, the results demonstrated that replacing the natural surfaces (NATURAL) of the ankle by artificial replicas (ANATOMICAL) did not significantly affect the range of motion of the ankle complex or its components, i.e. ankle and subtalar joints, nor do they affect the total laxity of the ankle complex in inversion/eversion or internal/external rotation. This high reliability, and lack of significant effects on either range of motion or total laxity, is an important finding proving that the combined factors involved in the process, such as replacing the natural surfaces with artificial replicas and the overall surgical procedure, do not significantly affect the mobility and stability characteristics of the ankle joint. The results of this study also demonstrate that the total laxity of the ankle complex in inversion/eversion and internal/external rotation decrease significantly when the ankle is in dorsiflexion compared to neutral while not significantly affected

when it is in plantarflexion (Table 2). This strong stiffening effect with dorsiflexion is expected given the geometry of the articulating surfaces. However, to the best of our knowledge, this phenomena has not been quantified in the past.

This study has several limitations. Although a small amount of compression was maintained at the ankle complex during the experiment, the kinematic and laxity characterization was performed under no external compressive loading. However, this was shown to be appropriate when the effect of the anatomical passive structures is the main scope of the analysis (Leardini et al., 1999). In addition, the present experimental validation was limited to the evaluation of the relative rotations between bones, whereas other kinematics characterizations, such as linear displacements and surface-to-surface joint motion, were not included at present. Finally, the size of the specimen population was limited to ten which may limit the statistical reliability of the results. This practical limitation was addressed using a repeated measure experimental design according to which each single specimen tested served as its own control thus greatly increasing the statistical reliability of the results. Finally, the order of testing of the three different conditions for all specimens was not randomized, starting with the NATURAL condition, then ANATOMICAL, and finishing with the SSCL set. Clearly the intact natural specimen had to be tested first, the ANATOMICAL set then followed since it provided an accurate template for positioning and securing the implants to the osteotomies. Once this was achieved, the SSCL used the same fixation sites for consistent accurate positioning and fixation.

In addition to establishing the reliability of the experimental technique, the results demonstrate that replacing the natural surfaces of the ankle joint by customized surfaces that correspond to a saddle shaped skewed truncated cone with the apex of the cone oriented laterally (Siegler et al., 2014), produce mobility and stability behavior similar to that of the ankle with natural surfaces. This is an important first step towards the development of a new TAR with articulating surfaces that represent proper functional morphology and producing close-to-natural mobility and stability behavior. Clearly, this study focused and was limited to the range of motion and total laxity behavior. Future studies are required to expand the technique to include additional factors such as load transfer including joint surface contact pressure, and full load- displacement characterization.

Conflict of interest

This is to certify that none of the authors have any conflict of interest with the subject matter of this manuscript.

Acknowledgments

This study was support by a grant from Coulter-Drexel Translational Research Partnership (Grant no. 282831).

References

Barnett, C.H., Napier, J.R., 1952. The axis of rotation at the ankle joint in man, Its influence upon the form of the talus and mobility of the fibula. J. Anat. 86, 1–9.
Belvedere, C., Ensini, A., Leardini, A., Bianchi, L., Catani, F., Giannini, S., 2007. Alignment of resection planes in total knee replacement obtained with the conventional technique, as assessed by a modern computer-based navigation system. Int. J. Med. Robot 3 (2), 117–124.
Belvedere, C., Ensini, A., Leardini, A., Dedda, V., Feliciangeli, A., Cenni, F., Timoncini, A., Barbadoro, P., Giannini, S., 2014. Tibio-femoral and patello-femoral joint kinematics during navigated total knee arthroplasty with patellar resurfacing. Knee Surg. Sport. Traumatol. Arthrosc. 22 (8), 1719–1727.
Cappozzo, A., Catani, F., Croce, U.D., Leardini, A., 1995. Position and orientation in space of bones during movement: anatomical frame definition and determination. Clin. Biomech. (Bristol, Avon) 10 (4), 171–178.
Close, J.R., 1956. Some applications of the functional anatomy of the ankle joint. J. Bone Jt. Surg. 38-A (4), 761–781.
Close, J.R., Inman, V.T., 1952. The action of the ankle joint. Prosthetic Devices Research Project, Institute of Engineering Research. University of California, Berkeley.
Coester, L.M., Saltzman, C.L., Leupold, J., Pontarelli, W., 2001. Long-term results following ankle arthrodesis for post-traumatic arthritis. J Bone Jt. Surg. Am. 83-A (2), 219–228.
Franci, R., Parenti-Castelli, V., Belvedere, C., Leardini, A., 2009. A new one-DOF fully parallel mechanism for modelling passive motion at the human tibiotalar joint. J Biomech. 42 (10), 1403–1408.
Giannini, S., Romagnoli, M., O'Connor, J.J., Malerba, F., Leardini, A., 2010. Total ankle replacement compatible with ligament function produces mobility, good clinical scores, and low complication rates: an early clinical assessment. Clin. Orthop. Relat. Res. 468 (10), 2746–2753.
Grood, E.S., Suntay, W.J., 1983. A joint coordinate system for the clinical description of three- dimensional motions: application to the knee. J. Biomech. Eng. 105 (2), 136–144.
Hicks, J.H., 1953. The mechanics of the foot I, the joints. J. Anat. 87, 345–357.
Hintermann, B., Valderrabano, V., Dereymaeker, G., Dick, W., 2004. The HINTEGRA ankle: rationale and short-term results of 122 consecutive ankles. Clin. Orthop. Relat. Res. 424, 57–68.
Imhauser, C.W., Abidi, N.A., Frankel, D.Z., Gavin, K., Siegler, S., 2002. Biomechanical evaluation of the efficacy of external stabilizers in the conservative treatment of acquired flatfoot deformity. Foot Ankle Int. 23 (8), 727–737.
Imhauser, C.W., Siegler, S., Udupa, J.K., Toy, J.R., 2008. Subject-specific models of the hindfoot reveal a relationship between morphology and passive mechanical properties. J. Biomech. 41 (6), 1341–1349.
Inman, V.T., 1976. The Joints of the Ankle. Williams&Wilkins, Baltimore.
Lapointe, S.J., Siegler, S., Hillstrom, H., Nobilini, R.R., Mlodzienski, A., Techner, L., 1997. Changes in the flexibility characteristics of the ankle complex due to damage to the lateral collateral ligaments: an in vitro and in vivo study. J. Orthop. Res. 15 (3), 331–341.
Leardini, A., O'Connor, J.J., Catani, F., Giannini, S., 1999. Kinematics of the human ankle complex in passive flexion; a single degree of freedom system. J. Biomech. 32 (2), 111–118.
Liu, W., Siegler, S., Techner, L., 2001. Quantitative measurement of ankle passive flexibility using an arthrometer on sprained ankles. Clin. Biomech. (Bristol, Avon) 16 (3), 237–244.
Lundberg, A., Svensson, O.K., Nemeth, G., Selvik, G., 1989. The axis of rotation of the ankle joint. J. Bone Jt. Surg. Br. 71 (1), 94–99.
Ringleb, S.I., Udupa, J.K., Siegler, S., Imhauser, C.W., Hirsch, B.E., Liu, J., Odhner, D., Okereke, E., Roach, N., 2005. The effect of ankle ligament damage and surgical reconstructions on the mechanics of the ankle and subtalar joints revealed by three-dimensional stress MRI. J. Orthop. Res. 23 (4), 743–749.
Sancisi, N., Baldisserri, B., Parenti-Castelli, V., Belvedere, C., Leardini, A., 2014. One-degree-of-freedom spherical model for the passive motion of the human ankle joint. Med. Biol. Eng. Comput. 52 (4), 363–373.
Sewell, R.B.S., 1904. A study of the Astragalus. J. Anatomocal Physiol., 38.
Siegler, S., Chen, J., Schneck, C.D., 1988. The three-dimensional kinematics and flexibility characteristics of the human ankle and subtalar joints–Part I: kinematics. J. Biomech. Eng. 110 (4), 364–373.
Siegler, S., Lapointe, S., Nobilini, R., Berman, A.T., 1996. A six-degrees-of-freedom instrumented linkage for measuring the flexibility characteristics of the ankle joint complex. J. Biomech. 29 (7), 943–947.
Siegler, S., Liu, W., Sennett, B., Nobilini, R.J., Dunbar, D., 1997. The three-dimensional passive support characteristics of ankle braces. J. Orthop. Sport. Phys. Ther. 26 (6), 299–309.
Siegler, S., Toy, J., Seale, D., Pedowitz, D., 2014. The Clinical Biomechanics Award 2013 – presented by the International Society of Biomechanics: new observations on the morphology of the talar dome and its relationship to ankle kinematics. Clin. Biomech. (Bristol, Avon) 29 (1), 1–6.
Siegler, S., Udupa, J.K., Ringleb, S.I., Imhauser, C.W., Hirsch, B.E., Odhner, D., Saha, P.K., Okereke, E., Roach, N., 2005. Mechanics of the ankle and subtalar joints revealed through a 3D quasi-static stress MRI technique. J. Biomech. 38 (3), 567–578.
Sparmann, M., Wolke, B., Czupalla, H., Banzer, D., Zink, A., 2003. Positioning of total knee arthroplasty with and without navigation support. A prospective, randomised study. J. Bone Jt. Surg. Br. 85 (6), 830–835.
Spirt, A.A., Assal, M., Hansen Jr., S.T., 2004. Complications and failure after total ankle arthroplasty. J. Bone Jt. Surg. Am. 86-A (6), 1172–1178.
Valderrabano, V., Hintermann, B., Nigg, B.M., Stefanyshyn, D., Stergiou, P., 2003a. Kinematic changes after fusion and total replacement of the ankle: part 1: range of motion. Foot Ankle Int. 24 (12), 881–887.
Valderrabano, V., Hintermann, B., Nigg, B.M., Stefanyshyn, D., Stergiou, P., 2003b. Kinematic changes after fusion and total replacement of the ankle: part 2: movement transfer. Foot Ankle Int. 24 (12), 888–896.
Valderrabano, V., Hintermann, B., Nigg, B.M., Stefanyshyn, D., Stergiou, P., 2003c. Kinematic changes after fusion and total replacement of the ankle: part 3: talar movement. Foot Ankle Int. 24 (12), 897–900.
Wood, P.L.R., Clough, T.M., Jari, S., 2000. Clinical comparison of two total ankle replacements. Foot Ankle Int. 21 (7), 546–550.